frontiers | Frontiers in Materials

TYPE Original Research
PUBLISHED 01 March 2024
DOI 10.3389/fmats.2024.1339865

OPEN ACCESS

EDITED BY
Luciano Feo,
University of Salerno, Italy

REVIEWED BY
Ömer Civalek,
Akdeniz University, Türkiye
Raffaele Barretta,
University of Naples Federico II, Italy
Giuseppe Lovisi,
University of Salerno, Italy

*CORRESPONDENCE
Li-Cai Zhao,
zhaolicai@tju.edu.cn
Kamran Asemi,
k.asemi@iau-tnb.ac.ir

RECEIVED 16 November 2023
ACCEPTED 07 February 2024
PUBLISHED 01 March 2024

CITATION
Zhang L-L, Zhao L-C, Lang S-J and Asemi K (2024), Free vibration analysis of functionally graded graphene platelet-reinforced metal foam doubly curved panel.
Front. Mater. 11:1339865.
doi: 10.3389/fmats.2024.1339865

Free vibration analysis of functionally graded graphene platelet-reinforced metal foam doubly curved panel

Li-Li Zhang[1], Li-Cai Zhao[2,3]*, Song-Jun Lang[1] and Kamran Asemi[4]*

[1]School of Engineering and Architecture, Chengdu Vocational and Technical College of Industry, Chengdu, Sichuan, China, [2]Department of Civil and Construction Engineering, National Taiwan University of Science and Technology, Taipei, Taiwan, [3]The Third Engineering Co., Ltd., China Railway 19th Bureau Group, Shenyang, Liaoning, China, [4]Department of Mechanical Engineering, Islamic Azad University, North Tehran Branch, Tehran, Iran

In this research, free vibration characteristics of functionally graded metal foam doubly curved panels reinforced with graphene platelets and with porosities have been surveyed. Halpin Tsai's approach is utilized for extracting the effective Young modulus of porous metal foam nanocomposite and also the effective density of nanocomposite porous doubly curved shell panel is estimated by using an extended rule of mixture. The FSDT hypothesis is utilized for determining the displacement field and the Finite element and Hamilton principle are utilized for deriving the mass and stiffness matrices of the structure. Finally, the influences of several variables such as porosity distribution, porosity coefficient, GPL dispersion pattern, the weight fraction of Nanofillers, and span angles on the free vibrations characteristics of doubly curved shell panels with FG porosities and reinforced by graphene platelet have been reported in detail.

KEYWORDS

Doubly curved panel, FG porous, GPLS, Free vibration, FSDT, FEM

1 Introduction

Composite materials, including functionally graded materials (FGMs), play a pivotal role in various industries due to their unique combination of properties, such as high strength-to-weight ratio and corrosion resistance (Hucke, 1971; Shen and Bever, 1972; Mahamood et al., 2017). The importance of composites lies in their ability to provide enhanced performance compared to traditional materials. To ensure their effectiveness, researchers employ rigorous evaluation methods to assess material properties. These methods include mechanical testing, non-destructive testing, and advanced analytical techniques (Voigt, 1889; Hill, 1965; Halpin and Tsai, 1969; Mori and Tanaka, 1973; Wakashima and Tsukamoto, 1991). Understanding and optimizing these properties are crucial for developing lightweight and durable structures in the aerospace, automotive, and construction industries. Researchers study composite structures (Wattanasakulpong and Chaikittiratana, 2015; Sobhani et al., 2021; Civalek et al., 2022) even in nanoscience (Saffari et al., 2017; Penna et al., 2021; Penna et al., 2022; Lovisi, 2023; Penna, 2023) to push the boundaries of material science, aiming for innovations that improve efficiency, sustainability, and

overall performance in diverse applications (Dastjerdi et al., 2020a; Dastjerdi et al., 2020b).

Nowadays, scholars are evaluating the performance of structures that are made of polymeric and metallic nanocomposite in practical applications subjected to various loadings. Also, some of these structures have been employed in various industries like aerospace, marine, automobile, etc. One of the most important characteristics of these structures is their low weight in connection with high stiffness. On the other hand, adding the nanoparticles to the matrix (polymer or metal) does not change the weight of the structure considerably but it can more significantly increase its stiffness. It is mentioned that these nanoparticles may decrease the stiffness of structures. Since, the nanoparticles have a high level of energy and if their weight fraction is more than a certain amount in the matrix, the nanoparticles stick together and agglomeration will occur. There are many investigations about determining the maximum weight fraction of various nanofillers. Two famous examples of nanoparticle reinforcement which recently attracted the attention of researchers are carbon nanotubes (CNTs) and graphene platelets (GPLs). Since many studies have been conducted into structures that are reinforced with these nanoparticles, studies are considered which are related to the free vibration characteristics of shell-type structures reinforced by GPLs. Babaei et al. (Mollaei et al., 2023) presented free vibrations of functionally graded graphene reinforced composite (FG-GPL RC) cylindrical shell panels employing three-dimensional FEM. Hamilton principle was applied to obtain the governing equations. Amirabadi et al. (Amirabadi et al., 2022) employed third-order shear deformation theory (TSDT) combined with generalized differential quadrature (GDQ) procedure to predict the free vibration behavior of rotating FG- GPL conical shells for various boundary conditions. Dynamic characteristics of FG-GPL shells with piezoelectric patches assuming nonlinear behavior for electro-elastic coupling were presented by Rao et al. (Rao et al., 2018). Nguyen Van Do and Hyung Lee (Van Do and Lee, 2020a) evaluated static bending and natural frequencies of FG-GPL RC cylindrical shell panels employing FSDT and utilizing the isogeometric method. Applying classical shell theory and the Rayleigh-Ritz technique, the free vibration response of sandwich FG-GPL cylindrical shells was studied by Permoon, Farsadi, and Askarian (Permoon et al., 2023). Dynamic characteristics of an FG-GPL conical structure applying Jacobi-Ritz solution were presented by Zhao et al. (Zhao et al., 2023). Free vibration characteristics of rotating 2D FG-GPL conical shells supporting an elastic medium employing FSDT were presented by Amirabadi et al. (Amirabadi et al., 2021). Mohammadi et al. (Mohammadi, 2023) applied isogeometric procedure and higher order shear deformation theory (HSDT) to evaluate free vibrations of trapezoidally corrugated FG-GPL RC laminated cylindrical panels. Mohammadi, Shojaei, and Kiani (Mohammadi et al., 2023) presented an isogeometric method for free vibrations of FG-GPL panel-type structures based on the Kirchhoff–Love shell hypothesis. Liu et al. employing an analytical model (Amirabadi et al., 2023) presented 3D buckling and free vibration behavior of pre-stressed FG-GPL RC cylinders. Dong et al. (Dong et al., 2022) combined GDQM and trigonometric expansion analysis to evaluate the vibration behavior of FG-GPL RC conical shells assuming the ring as a frequency controller based on FSDT. Dong et al. (Dong et al., 2018a) performed an investigation about the influences of rotation and axial force simultaneously on the geometrically nonlinear free vibrations of FG-GPL RC cylinders applying Donnell's theory and an analytical solution. Based on HSDT, the natural frequency characteristics of FG-GPL cylindrical and spherical shell-type panels by employing isogeometric solution were presented by Nguyen Van Do and Hyung Lee (Van Do and Lee, 2020b). Liu et al. (Liu et al., 2021) used three-dimensional elasticity assumptions and an analytical layer-wise solution for the investigation of free vibration characteristics of FG GPL spherical shells. Traveling wave evaluation of a rotating FG-GPL RC cylinder for several boundary conditions according to Donnell shell theory was conducted by Qin et al. (Qin et al., 2019). Utilizing FSDT as a theory and using GDQM as a solution, natural frequencies of FG-GPL cylinders resting on various types of elastic foundations for different BCs were presented by Sobhani et al. (Sobhani et al., 2023a). Sobhani and Avcar (Sobhani and Avcar, 2022) examined various nanofiller materials' effects on the free vibration of cylindrical shells employing FSDT and using GDQM as a numerical solution.

Free vibrations characteristic of FG-GPL doubly curved shell structures have been studied in few articles. The differences between these works are usually in methodology. In detail, Wang et al. (Wang et al., 2018) introduced an analytical model for obtaining natural frequencies of FG doubly curved panels reinforced by GPLs based on HSDT. Free vibration responses of FG GPLs doubly curved shells based on HSDT were presented by Adamian (Adamian et al., 2020). Employing FSDT and Ritz solution, free vibrations of FG-GPL doubly curved panels were presented by Esmaili et al. (Esmaeili et al., 2022). In another investigation by considering the same hypothesis and solution, they (Esmaeili and Kiani, 2022) studied thermal induced vibration responses of GPL RC doubly curved panels. Free vibrations of FG-GPL RC doubly curved shell-type structures in thermal conditions employing Reddy's HSDT and using an analytical model were developed by Shen et al. (Shen et al., 2019). Sobhi, Ashraf, and Zenkour (Sobhy and Zenkour, 2019) proposed an analytical model for free vibration analysis of FG-GPL RC doubly-curved panels supported on elastic foundations based on an HSDT.

The weight of the structure is too prominent in the aerospace industry and the low weight of the structure can be useful for other applications where saving energy is important. One of the ways to decrease the weight of a structure is BY creating pores in it; the stiffness of the structure also will decrease. To compensate for the decrease in stiffness of the structures, these structures can be reinforced with nanoparticles. Hence, scholars have examined the various types of structures which were fabricated by FG porous material reinforced by nanoparticles. Due to there being many investigations in this field, we review the articles which are related to the vibration behavior of shell structures made of FG porous material reinforced by GPLs. In detail, Bahaadini et al. (Bahaadini et al., 2019) proposed an analytical model for obtaining natural frequencies of FG-GPL RC conical shells with FG porosities employing Love's first approximation assumptions. Ye and Wang (Ye and Wang, 2021) employed the Galerkin method to study the resonance phenomenon in an FG- GPL cylinder with FG porosities based on Donnell's nonlinear assumptions. Wang et al. (Wang et al., 2019) conducted an investigation into the nonlinear vibrations of a porous cylinder reinforced with GPLs nanofillers by employing the Galerkin approach and Donnell nonlinear hypothesis. Moradi

Dastjerdi and Behdinan (Moradi-Dastjerdi and Behdinan, 2021) presented an axisymmetric meshless model according to moving least squares approximations for obtaining the stress waves in porous cylindrical shells reinforced by GPL nanofillers exposed to thermal conditions. Nonlinear free vibrations of FG-GPL imperfect cylinders with FG porosities employing FSDT were performed by means of an analytical model by Salehi et al. (Salehi et al., 2023). Nejadi et al. (Nejadi et al., 2021) presented a GDQM numerical model as a semi-analytical formulation for free vibrations of sandwich cylinders based on FSDT and by assuming porosity and GPL sense on transfering fluid flow. Zhou et al. (Zhou et al., 2021) employ Reddy theory and the standard Lagrange model to illustrate free vibrations of FG GPL cylinders with FG porosities under supersonic load. Ton-That et al. (Ton-That et al., 2021) reported the nonlinear forced vibrations of FG-GPL cylinders with FG porosity effects by applying nonlinear Donnell assumptions and the Galerkin solution. Ebrahimi et al. (Ebrahimi et al., 2019) presented an analytical model for free vibration analysis of FG –GPL cylinders with FG porosities employing the FSDT as a theory. Pourjabari et al. (Pourjabari et al., 2019) analytically reported the free and forced vibrations characteristic of the FG-GPL cylinders in a micro sense employing modified strain gradient theory. Free vibrations of FG-GPL cylinders considering various FG porosity patterns were presented by Barati and Zenkour (Barati and Zenkour, 2019). Kiarasi et al. (Kiarasi et al., 2021) utilized FEM as a numerical solution and two-dimensional axisymmetric elasticity as an accurate theory to study the free vibrations of FG-GPL RC joined conical–cylindrical structure considering FG porosities. Zhang et al. (Zhang et al., 2023) examined free vibrations characteristic of FG-GPL joined hemispherical–cylindrical–hemispherical structure with FG porosities by using 3D elasticity based on FEM. Cho (Cho, 2023) applied FSDT and two-dimensional FE solution to present free vibration characteristics of FG –GPL cylindrical panels with FG porosities. Twinkle and Pitchaimani (Twinkle and Pitchaimani, 2021) examined the influence of FG-GPL reinforcement and FG porosities on the free vibrations and stability of porous GPL-reinforced cylindrical shell panels according to HSDT and utilizing Galerkin solution. Salehi et al. (Salehi et al., 2023) proposed a novel analytical model for geometrically nonlinear vibrations of FG-GPL RC imperfect cylinders with FG porosities employing FSDT. A novel analytical model for investigating the traveling wave vibrations of rotating FG GPL joined conical-cylindrical structures considering FG porosities applying Donnell's assumptions was reported by Chai and Wang (Chai and Wang, 2022).

The above literature review shows that in the most of investigations, structures with simple shapes and governing equations like cylindrical and conical shells have been considered, and free vibrations of porous metal foam FG-GPL doubly curved panels have not been investigated so far. In this investigation, FSDT as a theory and FEM as a numerical solution are applied to investigate the natural frequency characteristics of porous FG-GPL metal foam doubly curved panels. Four distinct porosity distributions combined with five different GPL dispersion functions are assumed through the thickness of the structures. The porosity distributions are assumed with symmetric, asymmetric, and uniform patterns through the thickness of the structure. Two distributions of porosity are employed for a symmetric pattern. In one of them, the pores are mainly concentrated at the upper and lower surfaces of the doubly curved shell panel and in the other, the concentration of pores at the upper and lower surfaces of the structure is too low. In asymmetric porosity distribution, the number of pores at the structure's thickest point is low and the number of pores gradually increases from the structure's least to most thick points. Five distinct GPL dispersion functions are supposed via the thickness of the shell panel: GPLX, GPLO, GPLA, GPLV, and GPLUD. The effect of various variables including porosity distribution, porosity coefficient, GPL dispersion pattern, weight fraction of GPLs, and span angles on the free vibration characteristics of FG porous nanocomposite structure have been studied. In Section 2, the effective mechanical properties of the structure are presented by proposing the Halpin-Tsai model and extension rule of mixture. Then, in Section 3, the finite element procedure and Rayleigh-Ritz method are utilized for extracting the stiffness and mass matrix of FG porous doubly curved panel reinforced with GPLs.Finally, in Section 4 the numerical results of the natural frequencies of the structures are presented and discussed in detail. The most prominent finding results are presented in the conclusion section.

2 Governing equations of porous FG-GPL RC doubly curved shell panel

2.1 Description of the Geometry

Figure 1 denotes the geometrical parameters of the FG porous metal foam doubly-curved panel reinforced by GPLs, where h is the thickness of the shell structure, R_1 and R_2 are the radiuses of curvature, θ_1 and θ_2 represent the span angles of a doubly curved shell, respectively. Also, four distinct porosity patterns combined with five GPL dispersion functions are depicted in Figure 1.

2.2 Obtaining the equal mechanical properties of FG porous doubly curved panel reinforced with graphene platelet:

Four different porosity functions are supposed via the thickness of the doubly curved panel. (See Figure 1) and their relation to changing mechanical properties including Young modulus and density along the structure thickness is shown in Eqs 1–4. Besides, five GPL dispersion functions through the thickness of a doubly curved panel are shown in Figure 1; Eq. 16 (Anirudh et al., 2019; Li and Zheng, 2020; Moradi-Dastjerdi and Behdinan, 2020; Zhao et al., 2020).

Nonlinear symmetric porosity function 1:

$$\begin{cases} E(\Upsilon) = E^* \left[1 - e_0^1 \cos(\pi\Upsilon)\right] \\ G(\Upsilon) = G^* \left[1 - e_0^1 \cos(\pi\Upsilon)\right] \\ \rho(\Upsilon) = \rho^* \left[1 - e_0^1 \cos(\pi\Upsilon)\right] \end{cases} \quad (1)$$

where $\Upsilon = z/h$

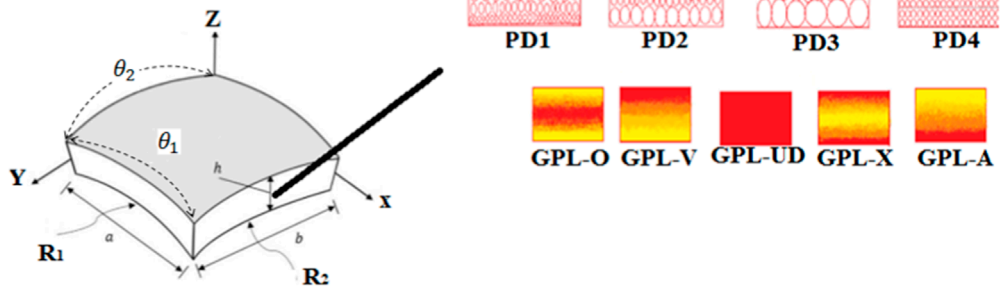

FIGURE 1
The schematic of FG porous nanocomposite doubly curved shell panel.

Nonlinear symmetric porosity function 2:

$$\begin{cases} E(\Upsilon) = E^*\left[e_0^2(1-\cos(\pi\Upsilon))\right] \\ G(\Upsilon) = G^*\left[e_0^2(1-\cos(\pi\Upsilon))\right] \\ \rho(\Upsilon) = \rho^*\left[e_m^2(1-\cos(\pi\Upsilon))\right] \end{cases} \tag{2}$$

Nonlinear asymmetric porosity function 3:

$$\begin{cases} E(\Upsilon) = E^*\left[e_0^3(1-\cos(\pi\Upsilon/2+\pi/4))\right] \\ G(\Upsilon) = G^*\left[e_0^3(1-\cos(\pi\Upsilon/2+\pi/4))\right] \\ \rho(\Upsilon) = \rho^*\left[e_m^3(1-\cos(\pi\Upsilon/2+\pi/4))\right] \end{cases} \tag{3}$$

Uniform porosity pattern 4:

$$\begin{cases} E = E^* e_0^4 \\ G = G^* e_0^4 \\ \rho = \rho^* e_m^4 \end{cases} \tag{4}$$

'Where E^*, G^*, and ρ^* are the corresponding material properties of nanocomposite doubly curved panels reinforced with GPL nanofillers but without internal cavities. Also, e_0^1, e_0^2,e_0^3, and e_0^4 (the amounts of them are between zero and one) represents the coefficients of porosity for distribution functions 1, 2, 3, and 4, respectively. e_m^1,e_m^2,e_m^3, and e_m^4 are related to the mass density coefficient for patterns 1, 2, 3, and 4, respectively.

Mass density and modules of elasticity for open-cell metal foam such as used in this research are dependent as presented in the below Eq. (Gibson and Ashby, 1982; Ashby et al., 2000; Asgari et al., 2022).

$$\frac{E(\Upsilon)}{E^*} = \left(\frac{\rho(\Upsilon)}{\rho^*}\right)^2 \tag{5}$$

Eq. 4 is utilized to denote the dependency between the mass density and porosity coefficients for each porosity function as following relations:

$$\begin{aligned} 1-e_m^1\cos(\pi\Upsilon) &= \sqrt{1-e_0^1 cos(\pi\Upsilon)} \\ e_m{}^2(1-\cos(\pi\Upsilon)) &= \sqrt{e_0^2(1-cos(\pi\Upsilon))} \\ e_m^3(1-\cos(\pi\Upsilon/2+pi/4)) &= \sqrt{e_0^3(1-\cos(\pi\Upsilon/2+pi/4))} \\ e_m^4 &= \sqrt{e_0^4} \end{aligned} \tag{6}$$

TABLE 1 Porosity coefficients for various patterns (Dong et al., 2018b; Yang et al., 2018).

e_0^1	e_0^2	e_0^3	e_0^4
0.1	0.1738	0.9361	0.0324
0.2	0.3442	0.8716	0.1176
0.3	0.5103	0.8064	0.1862
0.4	0.6708	0.7404	0.1501
0.5	0.8231	0.6733	0.2647
0.6	0.9612	0.6047	0.3364

For comparing the stiffness of different distributions, the analyses should be implemented for the shells with identical masses. Hence, it is supposed that the mass of doubly curved shell panels with different porosity functions and nanofiller dispersion functions are similar:

$$\begin{aligned} \int_{-h/2}^{h/2}\sqrt{1-e_0^1 cos(\pi\Upsilon)}\quad \mathrm{d}\Upsilon &= \int_{-h/2}^{h/2}\sqrt{e_0^2(1-cos(\pi\Upsilon))}\,d\Upsilon \\ &= \int_{-h/2}^{h/2}\sqrt{e_0^3(1-\cos(\pi\Upsilon/2+pi/4))}\,d\Upsilon = \sqrt{e_0^4} \end{aligned} \tag{7}$$

Based on Eq. 7, the amounts of e_0^2,e_0^3 and e_0^4 may be evaluated with a known value of e_0^1. Details of these coefficients are presented in Table 1. When e_0^1 reaches 0.6, e_0^2 (=0.9612) is near to the upper bound. This justifies the selection of $e_0^1 \in$ [0,0.6] hereafter.

The Young's modulus of the doubly curved panel fabricated by metallic nanocomposite without porosity based on the Halpin-Tsai micromechanics model (Choi and Lakes, 1995; Liu, 1997; Arshid et al., 2020; Arshid et al., 2021; Ebrahimi et al., 2021) is calculated as the following:

$$E^* = \frac{3}{8}\left(\frac{1+\varepsilon_L^{GPL}\eta_L^{GPL}V_{GPL}}{1-\eta_L^{GPL}V_{GPL}}\right)E_m + \frac{5}{8}\left(\frac{1+\varepsilon_W^{GPL}\eta_W^{GPL}V_{GPL}}{1-\eta_W^{GPL}V_{GPL}}\right) \quad (8)$$

in which

$$\varepsilon_L^{GPL} = \frac{2l_{GPL}}{t_{GPL}} \quad (9)$$

$$\varepsilon_W^{GPL} = \frac{2w_{GPL}}{t_{GPL}} \quad (10)$$

$$\eta_L^{GPL} = \frac{E_{GPL}-E_m}{E_{GPL}+\varepsilon_L^{GPL}E_m} \quad (11)$$

$$\eta_W^{GPL} = \frac{E_{GPL}-E_m}{E_{GPL}+\varepsilon_W^{GPL}E_m} \quad (12)$$

The mechanical properties of GPLs are shown with subscripts of GPL. Additionally, the subscripts of m are utilized for showing the corresponding mechanical properties of matrix material. The volume amount of nanofillers is indicated with V_{GPL}. l_{GPL}, w_{GPL}, and t_{GPL} symbols are hired for showing the length, width, and thickness of nanofillers, respectively (Arshid et al., 2020; Zhao et al., 2020; Ebrahimi et al., 2021).

According to the rule of mixture, mass density and Poisson's ratio of the shell are obtained as below Eqs (Guo et al., 2021; Babaei, 2022):

$$\rho^* = \rho_{GPL}V_{GPL} + \rho_m(1-V_{GPL}) \quad (13)$$

$$\nu^* = \nu_{GPL}V_{GPL} + \nu_m(1-V_{GPL}) \quad (14)$$

Accordingly, the shear modulus of the shell is expressed below:

$$G^* = \frac{E^*}{2(1+\nu^*)} \quad (15)$$

Also, the V_{GPL} for various GPL dispersion functions varies through the shell's thickness and may be obtained by using the below Eq (see also Figure 1):

$$V_{GPL}(z) = \begin{Bmatrix} t_{i1}[1-\cos(\pi\Upsilon)] & GPL-X \\ t_{i2}[\cos(\pi\Upsilon)] & GPL-O \\ t_{i3} & GPL-UD \\ t_{i4}\left[1-\cos\left(\frac{\pi}{4}-\frac{\pi}{2}\Upsilon\right)\right] & GPL-A \\ t_{i5}\left[\cos\left(\frac{\pi}{4}-\frac{\pi}{2}\Upsilon\right)\right] & GPL-V \end{Bmatrix} \quad (16)$$

Where $t_{i1}, t_{i2}, t_{i3}, t_{i4}$, and t_{i5} denote the upper limit of the V_{GPL}, and subscript i =1, 2, 3, and 4 denote corresponding parameters for porosity functions 1, 2, 3, and 4 within each pattern. V_{GPL}^T is the total volume amount of nanofillers and it is obtained by substituting the GPLs weight fraction Δ_{GPL} into Eq. 16. Hence, $t_{i1}, t_{i2}, t_{i3}, t_{i4}$, and t_{i5} may be obtained by Eq. 18 (Esmaeili et al., 2022).

$$V_{GPL}^T = \frac{\Delta_{GPL}\rho_m}{\Delta_{GPL}\rho_m + \rho_{GPL} - \Delta_{GPL}\rho_{GPL}} \quad (17)$$

$$V_{GPL}^T \int_{-h/2}^{h/2} \frac{\rho(\Upsilon)}{\rho_c} d\Upsilon = \begin{cases} t_{i1}\int_{-h/2}^{h/2}[1-\cos(\pi\Upsilon)]\frac{\rho(\varsigma\Upsilon)}{\rho_c}d\psi \\ t_{i2}\int_{-h/2}^{h/2}[\cos(\pi\Upsilon)]\frac{\rho(\Upsilon)}{\rho_c}d\psi \\ t_{i3}\int_{-h/2}^{h/2}\frac{\rho(\Upsilon)}{\rho_c}d\Upsilon \\ t_{i4}\int_{-h/2}^{h/2}\left[1-\cos\left(\frac{\pi}{4}-\frac{\pi}{2}\Upsilon\right)\right]\frac{\rho(\Upsilon)}{\rho_c}d\Upsilon \\ t_{i5}\int_{-h/2}^{h/2}\left[\cos\left(\frac{\pi}{4}-\frac{\pi}{2}\Upsilon\right)\right]\frac{\rho(\Upsilon)}{\rho_c}d\Upsilon \end{cases} \quad (18)$$

2.3 FSDT shell theory equations

FSDT shell theory is hired to present the displacements of doubly curved shell panels as follows:

$$\begin{aligned} u &= u_0 + z\ \alpha \\ v &= v_0 + z\beta \\ w &= w_0 \end{aligned} \quad (19)$$

In Eq. 2, u, v, and w, are displacements along the x, y, and z axes, respectively, while u_0, v_0, and w_0 are the same displacements at the mid-plane of the shell. Also, α and β are normal transverse rotations around y and x, respectively. Hence, the strain field of the doubly curved shell panel is as follows:

$$\begin{aligned} &\varepsilon_x = \varepsilon_x^0 + z\,k_x,\ \varepsilon_y = \varepsilon_y^0 + z\,k_y \\ &\gamma_{xy} = \gamma_{xy}^0 + z\,k_{xy},\ \gamma_{xz} = \gamma_{xz}^0,\ \gamma_{yz} = \gamma_{yz}^0 \end{aligned} \quad (20)$$

where

$$\begin{aligned} &\varepsilon_x^0 = \frac{\partial u_0}{\partial x} - \frac{w}{R_1},\quad \varepsilon_y^0 = \frac{\partial v_0}{\partial y} - \frac{w}{R_2} \\ &k_x = \frac{\partial \alpha}{\partial x},\ k_y = \frac{\partial \beta}{\partial y},\ k_{xy} = \frac{\partial \alpha}{\partial y} + \frac{\partial \beta}{\partial x} \\ &\gamma_{xz}^0 = \frac{\partial w}{\partial x} + \alpha,\ \gamma_{yz}^0 = \frac{\partial w}{\partial y} + \beta,\ \gamma_{xy}^0 = \frac{\partial v_0}{\partial x} + \frac{\partial u_0}{\partial y} - 2\frac{w}{R_{12}} \end{aligned} \quad (21)$$

Therefore, the matrix form of Eq. 21 will be as:

$$\begin{aligned} &\begin{bmatrix}\varepsilon_x \\ \varepsilon_y \\ \gamma_{xy}\end{bmatrix} = \begin{Bmatrix}\varepsilon_x^0 \\ \varepsilon_y^0 \\ \gamma_{xy}^0\end{Bmatrix} + z\begin{Bmatrix}k_x \\ k_y \\ k_{xy}\end{Bmatrix} = \begin{bmatrix} \frac{\partial}{\partial x} & 0 & -\frac{1}{R_1} & z\frac{\partial}{\partial x} & 0 \\ 0 & \frac{\partial}{\partial y} & -\frac{1}{R_2} & 0 & z\frac{\partial}{\partial y} \\ \frac{\partial}{\partial y} & \frac{\partial}{\partial x} & \frac{-2}{R_{12}} & \frac{\partial}{\partial y} & \frac{\partial}{\partial x} \end{bmatrix}\begin{bmatrix}u_0 \\ v_0 \\ w_0 \\ \alpha \\ \beta\end{bmatrix} = d_1 Q \\ &\begin{Bmatrix}\gamma_{xz}^0 \\ \gamma_{yz}^0\end{Bmatrix} = \begin{bmatrix} 0 & 0 & \frac{\partial}{\partial x} & 1 & 0 \\ 0 & 0 & \frac{\partial}{\partial y} & 0 & 1 \end{bmatrix}\begin{bmatrix}u_0 \\ v_0 \\ w_0 \\ \alpha \\ \beta\end{bmatrix} = d_2 Q \end{aligned} \quad (22)$$

where

10.3389/fmats.2024.1339865

TABLE 2 Comparison of results of present research with natural frequencies of ANSYS WORKBENCH.

ω (Hz)	ω_1	ω_2	ω_3	ω_4	ω_5	ω_6
ANSYS WORKBENCH	2719.1	3176.8	3616.5	3977.8	4157.4	4724.2
Present	2729.8	3188.7	3632.1	3990.1	4165.8	4738.4

TABLE 3 Natural frequencies of FG- porous doubly curved panel reinforced by graphene nanoparticles for various span angles and GPL pattern ($\theta_1 = 120°$, PD1,e_0=0.2, $\Delta_{GPL} = 0.05wt\%$).

GPL pattern	θ_2	λ_1	λ_2	λ_3	λ_4	λ_5	λ_6
GPL-X	*60°*	3396.1	3967.9	4517	4968.2	5192.6	5900.6
	90°	2784.2	3638.2	3673.8	3868.7	4308.5	4772.3
	150°	2408.1	3003.8	3123.5	3273.9	3424.2	3485.6
GPL-A	*60°*	3243.276	3769.505	4277.599	4670.108	4860.274	5493.459
	90°	2605.733	3387.164	3409.507	3563.846	3952.101	4354.151
	150°	2207.746	2739.466	2839.636	2954.367	3076.849	3115.29
GPL-V	*60°*	3214.086	3735.579	4239.101	4628.077	4816.531	5444.017
	90°	2582.281	3356.68	3378.821	3531.772	3916.532	4314.964
	150°	2187.876	2714.81	2814.08	2927.778	3049.158	3087.252
GPL-O	*60°*	3178.41	3694.115	4192.047	4576.706	4763.068	5383.589
	90°	2553.618	3319.421	3341.317	3492.57	3873.059	4267.068
	150°	2163.591	2684.676	2782.844	2895.28	3015.312	3052.984
GPL-UD	*60°*	3016.246	3505.64	3978.167	4343.2	4520.054	5108.916
	90°	2423.331	3150.063	3170.841	3314.377	3675.454	4049.36
	150°	2053.204	2547.703	2640.862	2747.562	2861.47	2897.22

$$Q = \begin{bmatrix} u_0 \\ v_0 \\ w_0 \\ \alpha \\ \beta \end{bmatrix},\ d_1 = \begin{bmatrix} \frac{\partial}{\partial x} & 0 & -\frac{1}{R_1} & z\frac{\partial}{\partial x} & 0 \\ 0 & \frac{\partial}{\partial y} & -\frac{1}{R_2} & 0 & z\frac{\partial}{\partial y} \\ \frac{\partial}{\partial y} & \frac{\partial}{\partial x} & \frac{-2}{R_{12}} & \frac{\partial}{\partial y} & \frac{\partial}{\partial x} \end{bmatrix},$$

$$d_2 = \begin{bmatrix} 0 & 0 & \frac{\partial}{\partial x} & 1 & 0 \\ 0 & 0 & \frac{\partial}{\partial y} & 0 & 1 \end{bmatrix}$$

$$\begin{Bmatrix} \varepsilon_x^0 \\ \varepsilon_y^0 \\ \gamma_{xy}^0 \end{Bmatrix} = \begin{bmatrix} \frac{\partial}{\partial x} & 0 & -\frac{1}{R_1} & 0 & 0 \\ 0 & \frac{\partial}{\partial y} & -\frac{1}{R_2}0 & 0 & 0 \\ \frac{\partial}{\partial y} & \frac{\partial}{\partial x} & \frac{-2}{R_{12}} & 0 & 0 \end{bmatrix} \begin{bmatrix} u_0 \\ v_0 \\ w_0 \\ \alpha \\ \beta \end{bmatrix} = d_3 Q$$

$$\begin{Bmatrix} k_x \\ k_y \\ k_{xy} \end{Bmatrix} = \begin{bmatrix} 0 & 0 & 0 & \frac{\partial}{\partial x} & 0 \\ 0 & 0 & 0 & 0 & \frac{\partial}{\partial y} \\ 0 & 0 & 0 & \frac{\partial}{\partial y} & \frac{\partial}{\partial x} \end{bmatrix} \begin{bmatrix} u_0 \\ v_0 \\ w_0 \\ \alpha \\ \beta \end{bmatrix} = d_4 Q$$

where

$$d_3 = \begin{bmatrix} \frac{\partial}{\partial x} & 0 & -\frac{1}{R_1} & 0 & 0 \\ 0 & \frac{\partial}{\partial y} & -\frac{1}{R_2}0 & 0 & 0 \\ \frac{\partial}{\partial y} & \frac{\partial}{\partial x} & \frac{-2}{R_{12}} & 0 & 0 \end{bmatrix},\ d_4 = \begin{bmatrix} 0 & 0 & 0 & \frac{\partial}{\partial x} & 0 \\ 0 & 0 & 0 & 0 & \frac{\partial}{\partial y} \\ 0 & 0 & 0 & \frac{\partial}{\partial y} & \frac{\partial}{\partial x} \end{bmatrix}$$

The constitutive relations of a porous FG-GPL doubly curved shell panel are:

TABLE 4 Natural frequencies of FG- porous doubly curved panel reinforced by graphene nanoparticles for various span angles and porosity distribution ($\theta_1 = 120°$, GPLX,e_0=0.2, $\Delta_{GPL} = 0.05wt\%$).

Porosity distribution	θ_2	λ_1	λ_2	λ_3	λ_4	λ_5	λ_6
PD1	*60°*	3396.1	3967.9	4517	4968.2	5192.6	5900.6
	90°	2784.2	3638.2	3673.8	3868.7	4308.5	4772.3
	150°	2408.1	3003.8	3123.5	3273.9	3424.2	3485.6
PD2	*60°*	2818.763	3269.55	3694.906	4029.21	4180.043	4720.48
	90°	2264.668	2937.919	2945.065	3074.765	3398.976	3741.483
	150°	1918.774	2376.126	2452.822	2548.928	2646.222	2676.941
PD3	*60°*	2377.27	2767.61	3087.37	3378.078	3507.134	3948.682
	90°	1909.961	2486.892	2460.821	2577.874	2851.804	3129.751
	150°	1618.243	2011.344	2049.516	2137.013	2220.229	2239.261
PD4	*60°*	2545.037	2936.762	3340.981	3661.563	3815.522	4305.078
	90°	2044.75	2638.886	2662.965	2794.207	3102.568	3412.233
	150°	1732.445	2134.274	2217.873	2316.35	2415.458	2441.37

TABLE 5 Natural frequencies of FG- porous doubly curved panel reinforced by graphene nanoparticles for various span angles and weight fraction of nanofiller ($\theta_1 = 120°$, GPLX, e_0=0.2, PD1).

Weight fraction of Nano-fillers (%wt) (%)	θ_2	λ_1	λ_2	λ_3	λ_4	λ_5	λ_6
0	*60°*	2207.465	2575.961	2932.436	3224.859	3320.668	3771.664
	90°	1911.075	2494.187	2518.593	2651.799	2909.582	3221.28
	150°	1691.425	2107.242	2191.215	2296.371	2366.272	2407.572
0.5	*60°*	3396.1	3967.9	4517	4968.2	5192.6	5900.6
	90°	2784.2	3638.2	3673.8	3868.7	4308.5	4772.3
	150°	2408.1	3003.8	3123.5	3273.9	3424.2	3485.6
1	*60°*	4007.398	4705.929	5379.747	5917.608	6185.472	7058.298
	90°	3446.338	4319.22	4379.871	4612.605	5137.456	5714.334
	150°	3066.041	3843.945	4013.975	4207.596	4401.174	4498.863

$$\begin{Bmatrix}\sigma_x\\ \sigma_y\\ \tau_{xy}\end{Bmatrix} = \begin{bmatrix}C_{11} & C_{12} & 0\\ C_{12} & C_{22} & 0\\ 0 & 0 & C_{66}\end{bmatrix}\begin{Bmatrix}\varepsilon_x\\ \varepsilon_y\\ \gamma_{xy}\end{Bmatrix}$$
$$\begin{Bmatrix}\tau_{xz}\\ \tau_{yz}\end{Bmatrix} = \begin{bmatrix}C_{44} & 0\\ 0 & C_{55}\end{bmatrix}\begin{Bmatrix}\gamma_{xz}\\ \gamma_{yz}\end{Bmatrix}$$
$$C_{11} = C_{22} = \frac{E^*}{1-\nu^{*2}}, C_{12} = \frac{\nu^* E^*}{1-\nu^{*2}}, C_{44} = C_{55} = C_{66} = G^* \quad (23)$$

By integrating the stress field along the thickness direction, resultant moment and force will be:

$$\begin{Bmatrix}N_x\\ N_y\\ N_{xy}\end{Bmatrix} = \int_{\frac{-h}{2}}^{\frac{h}{2}}\begin{bmatrix}\sigma_x\\ \sigma_y\\ \tau_{xy}\end{bmatrix}dz, \quad \begin{Bmatrix}M_x\\ M_y\\ M_{xy}\end{Bmatrix} = \int_{\frac{-h}{2}}^{\frac{h}{2}}\begin{bmatrix}\sigma_x\\ \sigma_y\\ \tau_{xy}\end{bmatrix}zdz$$
$$\begin{Bmatrix}Q_x\\ Q_y\end{Bmatrix} = \mathrm{K}^2\int_{\frac{-h}{2}}^{\frac{h}{2}}\begin{bmatrix}\tau_{xz}\\ \tau_{yz}\end{bmatrix}dz \quad (24)$$

In Eq. 24, K is the shear correction factor and equals 5/6.

TABLE 6 Natural frequencies of FG- porous doubly curved panel reinforced by graphene nanoparticles for various span angles and porosity coefficients ($\theta_1 = 120°$, GPLX, $\Delta_{GPL} = 0.05wt\%$, PD1).

e_0	θ_2	λ_1	λ_2	λ_3	λ_4	λ_5	λ_6
0.2	*60°*	3396.1	3967.9	4517	4968.2	5192.6	5900.6
	90°	2784.2	3638.2	3673.8	3868.7	4308.5	4772.3
	150°	2408.1	3003.8	3123.5	3273.9	3424.2	3485.6
0.4	*60°*	2818.763	3317.164	3789.763	4104.081	4273.51	4843.803
	90°	2357.104	3102.366	3143.965	3259.733	3616.813	3995.933
	150°	2054.687	2581.49	2693.994	2780.196	2897.024	2941.446
0.5	*60°*	2784.802	3225.903	3645.219	3985.49	4134.867	4669.145
	90°	2319.573	3005.182	3012.193	3153.127	3485.752	3836.742
	150°	2047.704	2532.447	2613.929	2723.497	2827.578	2860.207

Simplified form of Eq. 24 is as follows:

$$\begin{bmatrix} N_x \\ N_y \\ N_{xy} \\ M_x \\ M_y \\ M_{xy} \\ Q_x \\ Q_y \end{bmatrix} = \begin{bmatrix} A_{11} & A_{12} & 0 & B_{11} & B_{12} & 0 & 0 & 0 \\ A_{12} & A_{22} & 0 & B_{12} & B_{22} & 0 & 0 & 0 \\ 0 & 0 & A_{66} & 0 & 0 & B_{66} & 0 & 0 \\ B_{11} & B_{12} & 0 & D_{11} & D_{12} & 0 & 0 & 0 \\ B_{12} & B_{22} & 0 & D_{12} & D_{22} & 0 & 0 & 0 \\ 0 & 0 & B_{66} & 0 & 0 & D_{66} & 0 & 0 \\ 0 & 0 & 0 & 0 & 0 & 0 & K^2A_{44} & 0 \\ 0 & 0 & 0 & 0 & 0 & 0 & 0 & K^2A_{55} \end{bmatrix} \begin{Bmatrix} \varepsilon_x^0 \\ \varepsilon_y^0 \\ \gamma_{xy}^0 \\ k_x \\ k_y \\ k_{xy} \\ \gamma_{xz}^0 \\ \gamma_{yz}^0 \end{Bmatrix} \tag{25}$$

where:

$$\left(A_{ij}, B_{ij}, D_{ij}\right) = \int_{-\frac{h}{2}}^{\frac{h}{2}} C_{ij}\left(1, z, z^2\right) dz \tag{26}$$

The strain and kinetic energies of the doubly curved panel may be presented as the below Eqs.

$$\begin{aligned} \delta U = \delta U_1 &= \frac{1}{2}\iiint \varepsilon^T \sigma dV \\ &= \iint \begin{Bmatrix} N_x\varepsilon_x^0 + N_y\varepsilon_y^0 + N_{xy}\gamma_{xy}^0 + M_xK_x + M_yK_y + \\ M_{xy}K_{xy} + Q_x\gamma_{xz} + Q_y\gamma_{yz} \end{Bmatrix} \\ dxdy &= \int \left(\left((d_3Q)^TA^T + (d_4Q)^TB^T\right)(d_3\delta Q)\right) \\ &\quad + \left((d_3Q)^TB^T + (d_4Q)^TD^T\right)(d_4\delta Q) + (d_2Q)^Te^T \\ &\quad (d_2\delta Q)dxdy \\ \delta T &= \int_{-\frac{h}{2}}^{\frac{h}{2}} \rho(\ddot{u}\delta u + \ddot{v}\delta v + \ddot{w}\delta w)dV \end{aligned} \tag{27}$$

where:

$$\begin{cases} \delta u = \delta u_0 + z\delta_\alpha \\ \delta v = \delta v_0 + z\delta_\beta \\ \delta w = \delta w_0 \end{cases} \quad \begin{cases} \ddot{u} = \dfrac{\partial^2 u_0}{\partial t^2} + z\dfrac{\partial^2 \alpha}{\partial t^2} \\ \ddot{v} = \dfrac{\partial^2 v_0}{\partial t^2} + z\dfrac{\partial^2 \beta}{\partial t^2} \\ \ddot{w} = \dfrac{\partial^2 w_0}{\partial t^2} \end{cases} \tag{28}$$

$$\begin{aligned} \delta T = \int\int_{-\frac{h}{2}}^{\frac{h}{2}} \rho\Bigg(\left(\frac{\partial^2 u_0}{\partial t^2} + z\frac{\partial^2 \alpha}{\partial t^2}\right)\left(\delta u_0 + z\delta_\alpha\right)\Bigg) \\ + \left(\frac{\partial^2 v_0}{\partial t^2} + z\frac{\partial^2 \beta}{\partial t^2}\right)\left(\delta v_0 + z\delta_\beta\right) + \frac{\partial^2 w_0}{\partial t^2}\delta w_0 dzdA \end{aligned}$$

Replacing Eqs 27, 28 Hamilton's principle, we have:

$$\begin{aligned} \int_{t_1}^{t_2}\Bigg[\iint_{-\frac{h}{2}}^{\frac{h}{2}} \rho\Bigg(\left(\frac{\partial^2 u_0}{\partial t^2} + z\frac{\partial^2 \alpha}{\partial t^2}\right)\left(\delta u_0 + z\delta_\alpha\right)\Bigg)\Bigg] \\ + \left(\frac{\partial^2 v_0}{\partial t^2} + z\frac{\partial^2 \beta}{\partial t^2}\right)\left(\delta v_0 + z\delta_\beta\right) + \frac{\partial^2 w_0}{\partial t^2}\delta w_0 dzdA \\ + \int \Big(\left((d_3Q)^TA^T + (d_4Q)^TB^T\right)(d_3\delta Q) + \left((d_3Q)^TB^T + (d_4Q)^TD^T\right) \\ (d_4\delta Q) + (d_2Q)^Te^T(d_2\delta Q)dxdy\,dt = 0 \end{aligned} \tag{29}$$

2.4 FEM solution of governing equations:

In this section, for solving the governing motion equations of the shell, the graded FE method is used. In conventional FEM, the material property is constant through the element. In GFEM, to treat the material heterogeneity, in addition to the displacement field, the

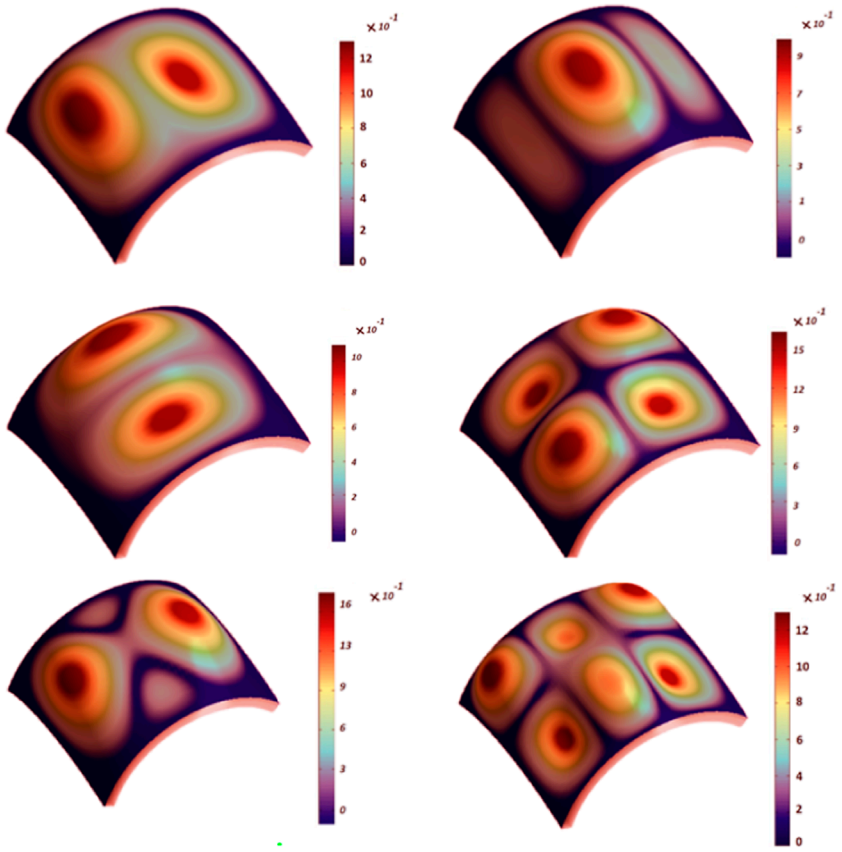

FIGURE 2
The first six mode shapes of FG-GPL porous doubly curved panel (GPLX, $\Delta_{GPL} = 0.05wt\%$, PD1, e0=0.2, R1=0.225 m, R2=0.4 m, $\theta_1 = 120^0, \theta_2 = 60^0$).

material properties of the FG-GPL porous doubly curved structure could also be determined from their nodal values. This approach leads to a smooth change of the properties along the structure and also obtains more precise results than discretizing the structure into elements with constant properties. By using the interpolation functions of cubic ten nodded triangular element, the displacement field, and material properties of individual element (e) in terms of the nodal displacement vector q, nodal elasticity modulus E_i and mass density ρ_i and shape function matrix Ψ are as:

$$Q^{(e)} = \left(\begin{pmatrix} \Psi_1 & \cdots & 0 \\ \vdots & \ddots & \vdots \\ 0 & \cdots & \Psi_1 \end{pmatrix} \cdots \begin{pmatrix} \Psi_{10} & \cdots & 0 \\ \vdots & \ddots & \vdots \\ 0 & \cdots & \Psi_{10} \end{pmatrix} \right) \begin{Bmatrix} u_{01} \\ v_{01} \\ w_{01} \\ \alpha_1 \\ \beta_1 \\ \vdots \\ u_{010} \\ v_{010} \\ w_{010} \\ \alpha_{10} \\ \beta_{10} \end{Bmatrix} = \Psi q(\mathrm{e}) \tag{30}$$

$$E^* = \sum_{i=1}^{10} E_i \psi_i = \Psi \Xi, \rho * = \sum_{i=1}^{10} \rho_i \psi_i = \Psi \Re$$

where $\Psi_n, \mathrm{n} = 1, 2, \ldots, 10$ are the approximation functions and presented in the Appendix. u_{0i}, v_{0i}, w_{0i}, α_i and β_i are nodal DOFs, Ξ and $\Re$ are respectively vectors containing elasticity modulus and mass density of each node, and are as:

$$\begin{aligned} \psi &= [\psi_1\ \psi_2\ \psi_3\ \psi_4\ \psi_5\ \psi_6\ \psi_7\ \psi_8\ \psi_9\ \psi_{10}], \\ \Xi &= [E_1\ E_2\ E_3\ E_4\ E_5\ E_6\ E_7\ E_8\ E_9\ E_{10}]^T \\ \Re &= [\rho_1\ \rho_2\ \rho_3\ \rho_4\ \rho_5\ \rho_6\ \rho_7\ \rho_8\ \rho_9\ \rho_{10}]^T \end{aligned} \tag{31}$$

Substituting Eqs 30, 31 in Eq. 29 can be rewritten as

$$\begin{aligned} \int_{\Omega_0^e} \Big[\big((d_3\Psi)^T A^T d_3\Psi + (d_4\Psi)^T B^T d_3\Psi + (d_3\Psi)^T B^T d_4\Psi \big) \Big] \\ + (d_4\Psi)^T D^T d_4\Psi + (d_2\Psi)^T e^T d_2\Psi q + \Psi^T I \Psi \ddot{q}\, dxdy = 0 \end{aligned} \tag{32}$$

where $d_2\Psi = B_2, d_3\Psi = B_3, d_4\Psi = B_4$.

$$\int_{\Omega_0^e} \Big[\big(B_3{}^T A^T B_3 + B_4{}^T B^T B_3 + B_3{}^T B^T B_4 + B_4{}^T D^T B_4 + B_2{}^T e^T B_2 \big) q + \Psi^T I \Psi \ddot{q} \Big] dxdy = 0 \tag{33}$$

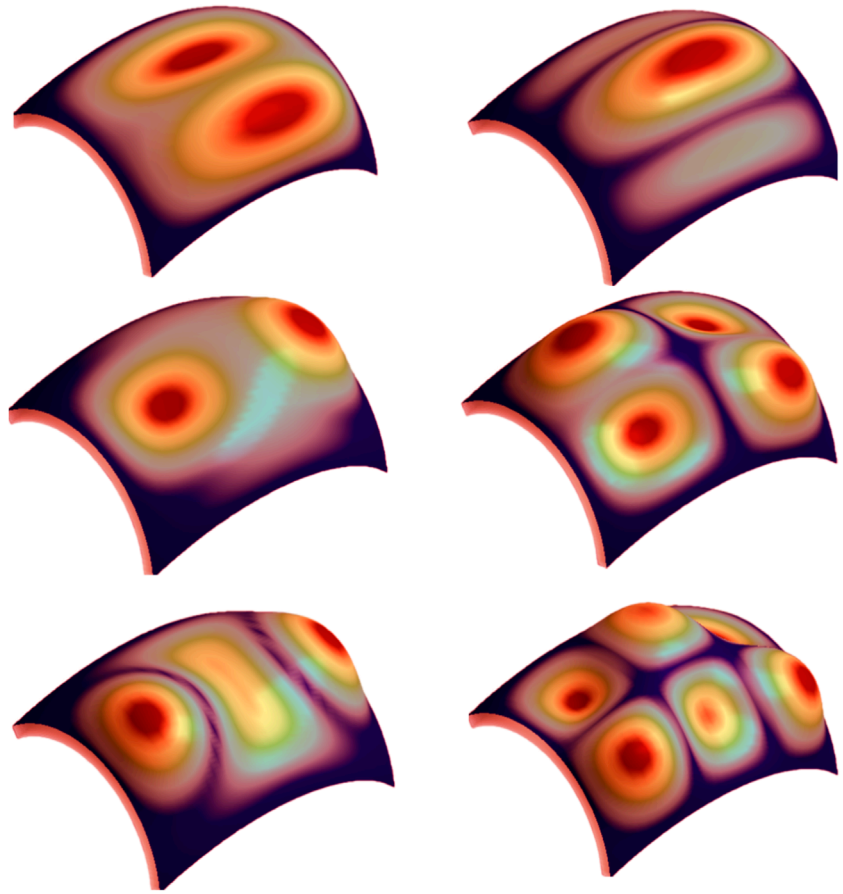

FIGURE 3
The first six mode shapes of FG-GPL porous doubly curved panel (GPLX, $\Delta_{GPL} = 0.05wt\%$, PD1, e0=0.2, R1=0.225 m, R2=0.4 m, $\theta_1 = 120^0, \theta_2 = 90^0$).

Rearranging Eq. 33, the FE model of porous FG-GPL RC doubly curved panel element will be as follows:

$$\begin{aligned}(k_1+k_2+k_3)^{(e)}q^{(e)}+M^e\ddot{q}^{(e)}&=0\\ k_1^e&=\int_{\Omega_0^e}\left[{B_3}^T A^T+{B_4}^T B^T\right]B_3\,dxdy\\ k_2^e&=\int_{\Omega_0^e}\left[{B_3}^T B^T+{B_4}^T D^T\right]B_4\,dxdy\\ k_3^e&=\int_{\Omega_0^e}\left[{B_2}^T e^T B_2\right]dxdy\\ M^e&=\int_{\Omega_0^e}\Psi^T I\Psi\,dxdy\end{aligned}\tag{34}$$

Where in Eq. 34 and mass matrix of element, [I] may be evaluated as:

$$\mathrm{I}=\begin{bmatrix}\mathrm{I}_0&0&0&\mathrm{I}_1&0\\0&\mathrm{I}_0&0&0&\mathrm{I}_1\\0&0&\mathrm{I}_0&0&0\\\mathrm{I}_1&0&0&\mathrm{I}_2&0\\0&\mathrm{I}_1&0&0&\mathrm{I}_2\end{bmatrix}\tag{35}$$

where $\mathrm{I}_i, \mathrm{i} = 0, 1, 2$ are

$$\begin{Bmatrix}\mathrm{I}_0\\\mathrm{I}_1\\\mathrm{I}_2\end{Bmatrix}=\int_{-\frac{h}{2}}^{\frac{h}{2}}\begin{Bmatrix}1\\z\\z^2\end{Bmatrix}\rho dz\tag{36}$$

By assembly of mass, stiffness, and force matrices of each element, the FE motion equations of the FG-GPL RC doubly curved panel are as

$$(k_1+k_2+k_3)q+M\ddot{q}=0\tag{37}$$

The natural frequency problem of the structure may be derived by the solution of the eigenvalue model as follows:

$$((k_1+k_2+k_3)-M\omega^2)q=0\tag{38}$$

where ω is the circular natural frequency and q is the mode shapes of free vibrations.

The shell is fully clamped at its all edges as:

$$u_0, v_0, w_0, \alpha, \beta = 0\tag{39}$$

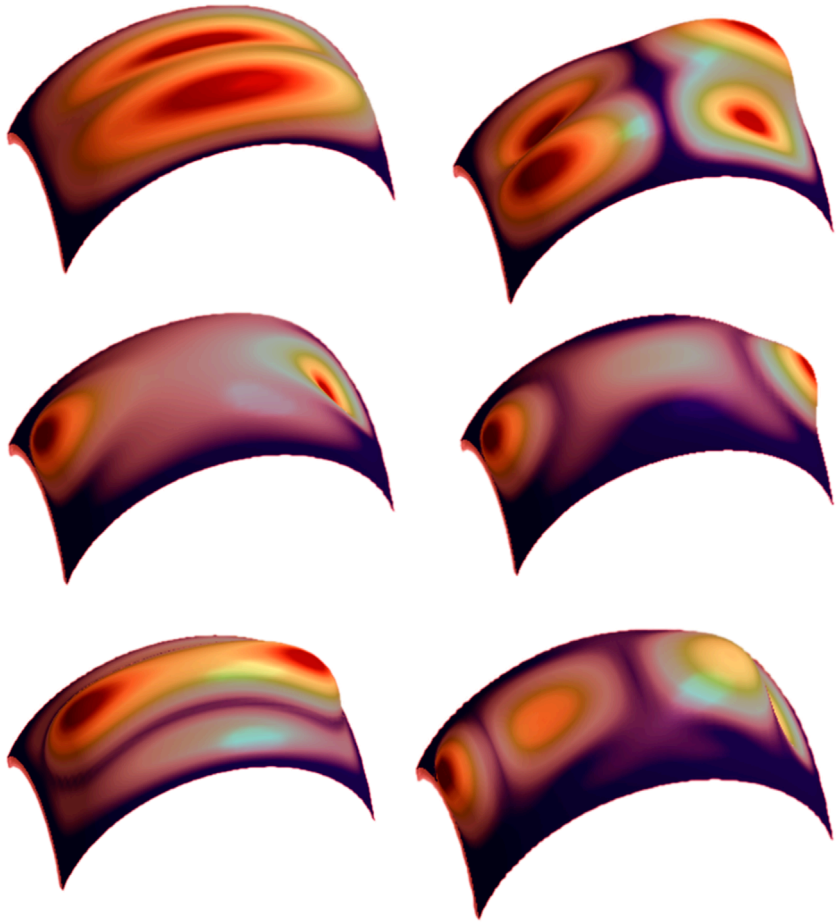

FIGURE 4
The first six buckling mode shapes of FG-GPL porous doubly curved panel (GPLX, Δ_{GPL} = 0.05*wt*%, PD1, e0=0.2, R1=0.225 m, R2=0.4 m, $\theta_1 = 120^0, \theta_2 = 150^0$).

3 Numerical results and discussion

In this part, natural frequencies of FG-GPL porous doubly curved shell panels examined by changing the volume weight fraction of nanofillers, nanofiller dispersion pattern, porosity distribution, and porosity coefficient are investigated in detail. The shell is fully clamped on its four edges.

3.1 Validation

To validate the obtained results of the present research, the first six natural frequencies of isotropic homogenous doubly curved shell panels with clamped edges are extracted employing commercial FEM software ANSYS-WORKBENCH, and the results are compared with the results of the present research. Therefore, one may consider e0=0 and $\Delta_{GPL} = 0wt\%$. Also, the dimensions and material properties of the shell are chosen as the following: Geometry: R1=0.225 m, R2=0.4 m, h=0.025m, $\theta_1 = 120°, \theta_2 = 60°$ and Mechanical properties: E=200 GPa, $\upsilon = 0.3, \rho = 7800 kg/m^3$

A comparison of the results of the present research with natural frequencies of ANSYS WORKBENCH is presented in Table 2, and it indicates excellent concordance between the results.

3.2 Natural frequencies of FG porous doubly curved shell panel reinforced by GPLs

The influence of coefficients of porosity and distributions of porosity, GPL pattern, and weight fraction of nanofillers and span angles on the natural frequency characteristics of an FG-GPL porous doubly curved shell panel is investigated in this section. Therefore, the below material properties and dimensions are employed:

Geometry: R1=0.225 m, R2=0.4 m, h=0.025m, $\theta_1 = 120°, \theta_2 = 60°$.

Material property: E_m = 130GPa, ρ_m = 8960 kg/m3, υ_m = 0.34 for copper[28], and E_{GPL} = 1.01 TPa, ρ_{GPL} = 1062.5 kg/m3, υ_{GPL} =0.186 , w_{GPL} = 1.5 μm, l_{GPL} = 2.5 μm, t_{GPL} = 1.5 nm for GPLs (Arshid et al., 2020; Zhao et al., 2020; Ebrahimi et al., 2021).

Table 3 describes the influences of nanofiller patterns on the free vibrations of the porous FG-GPL doubly curved shell panel ($\theta_1 = 120°$, PD1,e_0=0.2, $\Delta_{GPL} = 0.05wt\%$). As it is obvious in this

table, the maximum and minimum fundamental frequencies belong to GPLX and GPL-UD, respectively. Concentrating more nanofiller near the upper and lower surfaces of the doubly curved shell panel will result in more stiffness of the shell and consequently higher natural frequencies will be obtained. In addition, for uniform dispersion of nanofillers along the thickness of the structure, the minimum stiffness of the shell and also the lowest natural fundamental frequencies will be created. Also, the results of this table indicate that fundamental frequencies for GPL-A and GPL-V have approximately the same values. Comparing the results of Table 3 shows that the maximum difference between the fundamental frequencies with the change of nanofiller distributions is about 13%. In addition, the results of this table denote that by increasing the span angle θ_2 from *60* ° to *150* ° the natural frequency of the shell rose considerably, by 30%. This is due to the fact that by increasing the span angle, the ratio of stiffness to the mass of the shell increases. The influences of various porosity distributions are reported in Table 4 (θ_1 = 120°, GPLX,e_0=0.2, Δ_{GPL} = 0.05*wt*%). The maximum and minimum fundamental frequencies are estimated for PD1 and PD3, respectively. This means that PD1 provides higher rigidity for the shell while PD3 leads to a lower stiffness of the doubly curved shell panel. Comparing the results of Table 4 shows that the maximum difference between fundamental frequencies considering the effect of porosity distributions is about 43%. Also, the results of this table denote that when the distribution of pores is symmetric and their size is more around the mid-pane of the shell, the stiffness of the shell is greater and for the asymmetric distribution of pores, the stiffness of the shell will be lower. The impacts of the weight fraction of nanofillers on the natural frequencies of the porous FG-GPL structure (θ_1 = 120°, GPLX, e_0=0.2, PD1) is reported in Table 5. By changing the weight fraction of nanofillers from 0 to 1%, the fundamental frequencies of doubly curved shell panels considerably increase (approximately 80%). The impact of porosity coefficient on the free vibrations characteristics of porous FG-GPL doubly curved shell (θ_1 = 120°, GPLX, Δ_{GPL} = 0.05*wt*%, PD1) are indicated in Table 6. This table denotes that by increasing the porosity of the shell, the fundamental frequencies of FG-GPL porous doubly curved shell panels for PD1 decrease by approximately 22%. This is due to the fact that both the mass and stiffness of the structure decrease as the size of pores increases, the decrease of the mass of the shell is more remarkable than its stiffness. Comparing the results of Tables 3–6 illustrates that the natural frequencies are less influenced by GPL distribution than other parameters affecting the frequency of the shell. The first six free vibrations mode shapes of porous FG-GPL doubly curved shell panels for different span angles θ_2 = 60°, 90°, and 150° are shown in Figures 2–4. As it can be seen in these figures, it is obvious that by increasing the span angle of the doubly curved shell panel, higher free vibration mode shapes with more strain energies are obtained.

4 Conclusion

Free vibration characteristics of FG porous metal foam doubly curved shell panel reinforced by GPLs nanofillers have been surveyed in this research. Four distinct porosity functions and five GPL distributions are considered across the shell thickness. Applying FSDT and employing FEM based on the Hamilton principle, the governing motion equations of the shell are derived. The effects of GPL patterns, the weight fraction of nanofillers, porosity coefficient, and pattern and span angles on the free vibration responses of FG-GPL doubly curved panels with FG porosities have been examined. The main results are as:

a) Maximum and minimum fundamental frequencies are obtained for GPL-X and GPL-UD, respectively.
b) The fundamental frequencies of GPL-A and GPL-V are approximately identical.
c) The maximum and minimum fundamental frequencies of the shell have been obtained for PD1 and PD3.
d) By changing Δ_{GPL} from 0 to 1%, the fundamental frequencies of the structure remarkably increase (approximately 80%).
e) By growing the size of the porosity of the structure, the fundamental frequencies of the shell decrease by 22%.
f) The natural frequencies are less influenced by GPL distribution than other parameters (about 13%).
g) By increasing the span angle θ_2 from *60* ° to *150* °, the fundamental frequencies remarkably are enhanced by 30%.

Data availability statement

The raw data supporting the conclusion of this article will be made available by the authors, without undue reservation.

Author contributions

Li-Li Zhang: Conceptualization, Data curation, Formal Analysis, Investigation, Methodology, Software, Validation, Writing original draft, Writing–review & editing. Li-Cai Zhao: Conceptualization, Data curation, Formal Analysis, Investigation, Methodology, Software, Validation, Writing–original draft, Writing–review & editing. Song-Jun Lang: Conceptualization, Data curation, Formal Analysis, Investigation, Methodology, Software, Writing–original draft, Writing–review & editing. Kamran Asemi: Conceptualization, Investigation, Methodology, Supervision, Validation, Writing–review & editing.

Funding

The author(s) declare that no financial support was received for the research, authorship, and/or publication of this article.

Conflict of interest

Author L-CZ was employed by Co., Ltd. The remaining authors declare that the research was conducted in the absence of any commercial or financial relationships that could be construed as a potential conflict of interest.

Publisher's note

References

Adamian, A., Hosseini Safari, K., Sheikholeslami, M., Habibi, M., Al-Furjan, M. S. H., and Chen, G. (2020). Critical temperature and frequency characteristics of GPLs-reinforced composite doubly curved panel. *Appl. Sci.* 10 (9), 3251. doi:10.3390/app10093251

Amirabadi, H., Farhatnia, F., and Civalek, Ö. (2021). Frequency response of rotating two-directional functionally graded GPL-reinforced conical shells on elastic foundation. *J. Braz. Soc. Mech. Sci. Eng.* 43 (7), 349. doi:10.1007/s40430-021-03058-6

Amirabadi, H., Farhatnia, F., Eftekhari, S. A., and Hosseini-Ara, R. (2022). Free vibration analysis of rotating functionally graded GPL-reinforced truncated thick conical shells under different boundary conditions. *Mech. Based Des. Struct. Mach.* 50 (11), 3821–3852. doi:10.1080/15397734.2020.1822183

Amirabadi, H., Farhatnia, F., Eftekhari, S. A., and Hosseini-Ara, R. (2023). Wave propagation in rotating functionally graded GPL-reinforced cylindrical shells based on the third-order shear deformation theory. *Waves Random Complex Media* 33 (2), 345–371. doi:10.1080/17455030.2021.1880031

Anirudh, B., Ganapathi, M., Anant, C., and Polit, O. (2019). A comprehensive analysis of porous graphene-reinforced curved beams by finite element approach using higher-order structural theory: bending, vibration and buckling. *Compos. Struct.* 222, 110899. doi:10.1016/j.compstruct.2019.110899

Arshid, E., Amir, S., and Loghman, A. (2020). Static and dynamic analyses of FG-GNPs reinforced porous nanocomposite annular micro-plates based on MSGT. *Int. J. Mech. Sci.* 180, 105656. doi:10.1016/j.ijmecsci.2020.105656

Arshid, E., Amir, S., and Loghman, A. (2021). Thermal buckling analysis of FG graphene nanoplatelets reinforced porous nanocomposite MCST-based annular/circular microplates. *Aerosp. Sci. Technol.* 111, 106561. doi:10.1016/j.ast.2021.106561

Asgari, G. R., Arabali, A., Babaei, M., and Asemi, K. (2022). Dynamic instability of sandwich beams made of isotropic core and functionally graded graphene platelets-reinforced composite face sheets. *Int. J. Struct. Stab. Dyn.* 22 (08), 2250092. doi:10.1142/s0219455422500924

Ashby, M. F., Evans, T., Fleck, N. A., Hutchinson, J., Wadley, H., and Gibson, L. (2000). *Metal foams: a design guide*. Oxford, United Kingdom: Butterworth-Heinemann.

Babaei, H. (2022). Thermomechanical analysis of snap-buckling phenomenon in long FG-CNTRC cylindrical panels resting on nonlinear elastic foundation. *Compos. Struct.* 286, 115199. doi:10.1016/j.compstruct.2022.115199

Bahaadini, R., Saidi, A. R., Arabjamaloei, Z., and Ghanbari-Nejad-Parizi, A. (2019). Vibration analysis of functionally graded graphene reinforced porous nanocomposite shells. *Int. J. Appl. Mech.* 11 (07), 1950068. doi:10.1142/s1758825119500686

Barati, M. R., and Zenkour, A. M. (2019). Vibration analysis of functionally graded graphene platelet reinforced cylindrical shells with different porosity distributions. *Mech. Adv. Mater. Struct.* 26 (18), 1580–1588. doi:10.1080/15376494.2018.1444235

Chai, Q., and Wang, Y. Q. (2022). Traveling wave vibration of graphene platelet reinforced porous joined conical-cylindrical shells in a spinning motion. *Eng. Struct.* 252, 113718. doi:10.1016/j.engstruct.2021.113718

Cho, J. R. (2023). Free vibration analysis of functionally graded porous cylindrical panels reinforced with graphene platelets. *Nanomaterials* 13 (9), 1441. doi:10.3390/nano13091441

Choi, J., and Lakes, R. (1995). Analysis of elastic modulus of conventional foams and of re-entrant foam materials with a negative Poisson's ratio. *Int. J. Mech. Sci.* 37, 51–59. doi:10.1016/0020-7403(94)00047-n

Civalek, Ö., Dastjerdi, S., and Akgöz, B. (2022). Buckling and free vibrations of CNT-reinforced cross-ply laminated composite plates. *Mech. Based Des. Struct. Mach.* 50 (6), 1914–1931. doi:10.1080/15397734.2020.1766494

Dastjerdi, S., Akgöz, B., and Civalek, Ö. (2020a). On the effect of viscoelasticity on behavior of gyroscopes. *Int. J. Eng. Sci.* 149, 103236. doi:10.1016/j.ijengsci.2020.103236

Dastjerdi, S., Akgöz, B., Civalek, Ö., Malikan, M., and Eremeyev, V. A. (2020b). On the non-linear dynamics of torus-shaped and cylindrical shell structures. *Int. J. Eng. Sci.* 156, 103371. doi:10.1016/j.ijengsci.2020.103371

Dong, Y., Gao, Y., Zhu, Q., Moradi, Z., and Safa, M. (2022). TE-GDQE implementation to investigate the vibration of FG composite conical shells considering a frequency controller solid ring. *Eng. Analysis Bound. Elem.* 138, 95–107. doi:10.1016/j.enganabound.2022.01.017

Dong, Y. H., He, L. W., Wang, L., Li, Y. H., and Yang, J. (2018b). Buckling of spinning functionally graded graphene reinforced porous nanocomposite cylindrical shells: an analytical study. *Aerosp. Sci. Technol.* 82, 466–478. doi:10.1016/j.ast.2018.09.037

Dong, Y. H., Zhu, B., Wang, Y., Li, Y. H., and Yang, J. (2018a). Nonlinear free vibration of graded graphene reinforced cylindrical shells: effects of spinning motion and axial load. *J. Sound Vib.* 437, 79–96. doi:10.1016/j.jsv.2018.08.036

Ebrahimi, F., Mohammadi, K., Barouti, M. M., and Habibi, M. (2021). Wave propagation analysis of a spinning porous graphene nanoplatelet-reinforced nanoshell. *Waves random complex media* 31 (6), 1655–1681. doi:10.1080/17455030.2019.1694729

Ebrahimi, F., Seyfi, A., Dabbagh, A., and Tornabene, F. (2019). Wave dispersion characteristics of porous graphene platelet-reinforced composite shells. *Struct. Eng. Mech. Int'l J.* 71 (1), 99–107. doi:10.12989/sem.2019.71.1.099

Esmaeili, H. R., and Kiani, Y. (2022). Vibrations of graphene platelet reinforced composite doubly curved shells subjected to thermal shock. *Mech. Based Des. Struct. Mach.* 52, 650–679. doi:10.1080/15397734.2022.2120499

Esmaeili, H. R., Kiani, Y., and Beni, Y. T. (2022). Vibration characteristics of composite doubly curved shells reinforced with graphene platelets with arbitrary edge supports. *Acta Mech.* 233 (2), 665–683. doi:10.1007/s00707-021-03140-z

Gibson, I. J., and Ashby, M. F. (1982). The mechanics of three-dimensional cellular materials. *Proc. R. Soc. Lond. A. Math. Phys. Sci.* 382 (1782), 43–59. doi:10.1098/rspa.1982.0088

Guo, H., Yang, T., Żur, K. K., Reddy, J. N., and Ferreira, A. J. M. (2021). "Effect of thermal environment on nonlinear flutter of laminated composite plates reinforced with graphene nanoplatelets," in *Modeling and computation in vibration problems, volume 1: numerical and semi-analytical methods* (Bristol, United Kingdom: IOP Publishing).

Halpin, J. C., and Tsai, S. W. (1969). *Effects of environmental factors on composite materials*.

Hill, R. (1965). A self-consistent mechanics of composite materials. *J. Mech. Phys. Solids* 13 (4), 213–222. doi:10.1016/0022-5096(65)90010-4

Hucke, E. E. (1971). "Preliminary reports," in Memoranda and Technical Notes of the ARPA Materials Summer Conference Held at Woods Hole Volume 1, Massachusetts, July 1971. & MICHIGAN UNIV ANN ARBOR DEPT OF MATERIALS AND METALLURGICAL ENGINEERING.

Kiarasi, F., Babaei, M., Mollaei, S., Mohammadi, M., and Asemi, K. (2021). Free vibration analysis of FG porous joined truncated conical-cylindrical shell reinforced by graphene platelets. *Adv. nano Res.* 11 (4), 361–380. doi:10.12989/anr.2021.11.4.361

Li, Z., and Zheng, J. (2020). Nonlinear stability of the encased functionally graded porous cylinders reinforced by graphene nanofillers subjected to pressure loading under thermal effect. *Compos. Struct.* 233, 111584. doi:10.1016/j.compstruct.2019.111584

Liu, D., Zhou, Y., and Zhu, J. (2021). On the free vibration and bending analysis of functionally graded nanocomposite spherical shells reinforced with graphene nanoplatelets: three-dimensional elasticity solutions. *Eng. Struct.* 226, 111376. doi:10.1016/j.engstruct.2020.111376

Liu, G. R. (1997). A step-by-step method of rule-of-mixture of fiber-and particle-reinforced composite materials. *Compos. Struct.* 40 (3-4), 313–322. doi:10.1016/s0263-8223(98)00033-6

Lovisi, G. (2023). Application of the surface stress-driven nonlocal theory of elasticity for the study of the bending response of FG cracked nanobeams. *Compos. Struct.* 324, 117549. doi:10.1016/j.compstruct.2023.117549

Mahamood, R. M., Akinlabi, E. T., Mahamood, R. M., and Akinlabi, E. T. (2017). Types of functionally graded materials and their areas of application. *Funct. graded Mater.*, 9–21. doi:10.1007/978-3-319-53756-6_2

Mohammadi, H. (2023). "Isogeometric free vibration analysis of trapezoidally corrugated FG-GRC laminated panels using higher-order shear deformation theory," in *Structures (vol. 48)* (Amsterdam, Netherlands: Elsevier), 642–656.

Mohammadi, H., Shojaee, M., and Kiani, Y. (2023). A simplified isogeometric approach for vibrational analysis of nanocomposite panels with a free-form curve. *Thin-Walled Struct.* 183, 110426. doi:10.1016/j.tws.2022.110426

Mollaei, S., Babaei, M., and Asemi, K. (2023). Torsional buckling of functionally graded graphene reinforced composite laminated cylindrical panel. *Archive Appl. Mech.* 93 (2), 427–435. doi:10.1007/s00419-022-02132-2

Moradi-Dastjerdi, R., and Behdinan, K. (2020). Stability analysis of multifunctional smart sandwich plates with graphene nanocomposite and porous layers. *Int. J. Mech. Sci.* 167, 105283. doi:10.1016/j.ijmecsci.2019.105283

Moradi-Dastjerdi, R., and Behdinan, K. (2021). Stress waves in thick porous graphene-reinforced cylinders under thermal gradient environments. *Aerosp. Sci. Technol.* 110, 106476. doi:10.1016/j.ast.2020.106476

Mori, T., and Tanaka, K. (1973). Average stress in matrix and average elastic energy of materials with misfitting inclusions. *Acta metall.* 21 (5), 571–574. doi:10.1016/0001-6160(73)90064-3

Nejadi, M. M., Mohammadimehr, M., and Mehrabi, M. (2021). Free vibration and stability analysis of sandwich pipe by considering porosity and graphene platelet effects on conveying fluid flow. *Alexandria Eng. J.* 60 (1), 1945–1954. doi:10.1016/j.aej.2020.11.042

Penna, R. (2023). Bending analysis of functionally graded nanobeams based on stress-driven nonlocal model incorporating surface energy effects. *Int. J. Eng. Sci.* 189, 103887. doi:10.1016/j.ijengsci.2023.103887

Penna, R., Feo, L., and Lovisi, G. (2021). Hygro-thermal bending behavior of porous FG nano-beams via local/nonlocal strain and stress gradient theories of elasticity. *Compos. Struct.* 263, 113627. doi:10.1016/j.compstruct.2021.113627

Penna, R., Feo, L., Lovisi, G., and Fabbrocino, F. (2022). Application of the higher-order Hamilton approach to the nonlinear free vibrations analysis of porous FG nano-beams in a hygrothermal environment based on a local/nonlocal stress gradient model of elasticity. *Nanomaterials* 12 (12), 2098. doi:10.3390/nano12122098

Permoon, M. R., Farsadi, T., and Askarian, A. R. (2023). Vibration analysis of sandwich cylindrical shells made of graphene platelet polymer–viscoelastic–ceramic/metal FG layers. *Funct. Compos. Struct.* 5 (1), 015004. doi:10.1088/2631-6331/acbd28

Pourjabari, A., Hajilak, Z. E., Mohammadi, A., Habibi, M., and Safarpour, H. (2019). Effect of porosity on free and forced vibration characteristics of the GPL reinforcement composite nanostructures. *Comput. Math. Appl.* 77 (10), 2608–2626. doi:10.1016/j.camwa.2018.12.041

Qin, Z., Safaei, B., Pang, X., and Chu, F. (2019). Traveling wave analysis of rotating functionally graded graphene platelet reinforced nanocomposite cylindrical shells with general boundary conditions. *Results Phys.* 15, 102752. doi:10.1016/j.rinp.2019.102752

Rao, M. N., Schmidt, R., and Schröder, K. U. (2018). "Forced vibration analysis of FG-graphene platelet reinforced polymer composite shells bonded with piezoelectric layers considering electroelastic nonlinearities," in *Smart materials, adaptive structures and intelligent systems (vol. 51944, p. V001T03A006)* (American Society of Mechanical Engineers).

Saffari, S., Hashemian, M., and Toghraie, D. (2017). Dynamic stability of functionally graded nanobeam based on nonlocal Timoshenko theory considering surface effects. *Phys. B Condens. Matter* 520, 97–105. doi:10.1016/j.physb.2017.06.029

Salehi, M., Gholami, R., and Ansari, R. (2023). Analytical solution approach for nonlinear vibration of shear deformable imperfect FG-GPLR porous nanocomposite cylindrical shells. *Mech. Based Des. Struct. Mach.* 51 (4), 2177–2199. doi:10.1080/15397734.2021.1891096

Shen, H. S., Xiang, Y., and Fan, Y. (2019). Large amplitude vibration of doubly curved FG-GRC laminated panels in thermal environments. *Nanotechnol. Rev.* 8 (1), 467–483. doi:10.1515/ntrev-2019-0042

Shen, M., and Bever, M. B. (1972). Gradients in polymeric materials. *J. Mater. Sci.* 7, 741–746. doi:10.1007/bf00549902

Sobhani, E., Arbabian, A., Civalek, Ö., and Avcar, M. (2021). The free vibration analysis of hybrid porous nanocomposite joined hemispherical–cylindrical–conical shells. *Eng. Comput.* 38, 3125–3152. doi:10.1007/s00366-021-01453-0

Sobhani, E., and Avcar, M. (2022). The influence of various nanofiller materials (CNTs, GNPs, and GOPs) on the natural frequencies of Nanocomposite Cylindrical Shells: a comparative study. *Mater. Today Commun.* 33, 104547. doi:10.1016/j.mtcomm.2022.104547

Sobhani, E., Koohestani, M., Civalek, Ö., and Avcar, M. (2023a). Natural frequency investigation of graphene oxide powder nanocomposite cylindrical shells surrounded by Winkler/Pasternak/Kerr elastic foundations with a focus on various boundary conditions. *Eng. Analysis Bound. Elem.* 149, 38–51. doi:10.1016/j.enganabound.2023.01.012

Sobhani, E., Masoodi, A. R., and Civalek, Ö. (2023b). On vibrational-based numerical simulation of a jet engine cowl shell-like structure. *Mech. Adv. Mater. Struct.* 30 (19), 4016–4027. doi:10.1080/15376494.2022.2087241

Sobhy, M., and Zenkour, A. M. (2019). Vibration analysis of functionally graded graphene platelet-reinforced composite doubly-curved shallow shells on elastic foundations. *Steel compos. Struct.* 33 (2), 195–208. doi:10.12989/scs.2019.33.2.195

Ton-That, H. L., Nguyen-Van, H., and Chau-Dinh, T. (2021). A novel quadrilateral element for analysis of functionally graded porous plates/shells reinforced by graphene platelets. *Archive Appl. Mech.* 91, 2435–2466. doi:10.1007/s00419-021-01893-6

Twinkle, C. M., and Pitchaimani, J. (2021). Free vibration and stability of graphene platelet reinforced porous nano-composite cylindrical panel: influence of grading, porosity and non-uniform edge loads. *Eng. Struct.* 230, 111670. doi:10.1016/j.engstruct.2020.111670

Van Do, V. N., and Lee, C. H. (2020a). Bézier extraction based isogeometric analysis for bending and free vibration behavior of multilayered functionally graded composite cylindrical panels reinforced with graphene platelets. *Int. J. Mech. Sci.* 183, 105744. doi:10.1016/j.ijmecsci.2020.105744

Van Do, V. N., and Lee, C. H. (2020b). Static bending and free vibration analysis of multilayered composite cylindrical and spherical panels reinforced with graphene platelets by using isogeometric analysis method. *Eng. Struct.* 215, 110682. doi:10.1016/j.engstruct.2020.110682

Voigt, W. (1889). Ueber die Beziehung zwischen den beiden Elasticitätsconstanten isotroper Körper. *Ann. Phys.* 274 (12), 573–587. doi:10.1002/andp.18892741206

Wakashima, K., and Tsukamoto, H. (1991). Mean-field micromechanics model and its application to the analysis of thermomechanical behaviour of composite materials. *Mater. Sci. Eng. A* 146 (1-2), 291–316. doi:10.1016/0921-5093(91)90284-t

Wang, A., Chen, H., Hao, Y., and Zhang, W. (2018). Vibration and bending behavior of functionally graded nanocomposite doubly-curved shallow shells reinforced by graphene nanoplatelets. *Results Phys.* 9, 550–559. doi:10.1016/j.rinp.2018.02.062

Wang, Y. Q., Ye, C., and Zu, J. W. (2019). Nonlinear vibration of metal foam cylindrical shells reinforced with graphene platelets. *Aerosp. Sci. Technol.* 85, 359–370. doi:10.1016/j.ast.2018.12.022

Wattanasakulpong, N., and Chaikittiratana, A. (2015). Flexural vibration of imperfect functionally graded beams based on Timoshenko beam theory: Chebyshev collocation method. *Meccanica* 50, 1331–1342. doi:10.1007/s11012-014-0094-8

Yang, J., Chen, D., and Kitipornchai, S. (2018). Buckling and free vibration analyses of functionally graded graphene reinforced porous nanocomposite plates based on Chebyshev-Ritz method. *Compos. Struct.* 193, 281–294. doi:10.1016/j.compstruct.2018.03.090

Ye, C., and Wang, Y. Q. (2021). Nonlinear forced vibration of functionally graded graphene platelet-reinforced metal foam cylindrical shells: internal resonances. *Nonlinear Dyn.* 104 (3), 2051–2069. doi:10.1007/s11071-021-06401-7

Zhang, D., Wang, Y., and Li, L. (2023). Free vibration response of FG porous joined hemispherical–cylindrical–hemispherical shell vessels reinforced by graphene platelet. *Int. J. Struct. Stab. Dyn.* 23 (03), 2350025. doi:10.1142/s0219455423500256

Zhao, J., Fan, G., Guan, J., Li, H., Liu, J., Xie, Z., et al. (2023). Free vibration and dynamic analysis on free-constrained layer of graphene based on composite conical shell via Jacobi-Ritz method. *Int. J. Struct. Stab. Dyn*. doi:10.1142/s0219455424500238

Zhao, S., Yang, Z., Kitipornchai, S., and Yang, J. (2020). Dynamic instability of functionally graded porous arches reinforced by graphene platelets. *Thin-Walled Struct.* 147, 106491. doi:10.1016/j.tws.2019.106491

Zhou, X., Wang, Y., and Zhang, W. (2021). Vibration and flutter characteristics of GPL-reinforced functionally graded porous cylindrical panels subjected to supersonic flow. *Acta Astronaut.* 183, 89–100. doi:10.1016/j.actaastro.2021.03.003

10.3389/fmats.2024.1339865

Appendix A

$$\psi_1 = \frac{(x_{23}(y-y_3)-y_{23}(x-x_3))(x_{49}(y-y_9)-y_{49}(x-x_9))(x_{58}(y-y_8)-y_{58}(x-x_8))}{(x_{23}y_{13}-y_{23}x_{13})(x_{49}y_{16}-y_{49}x_{16})(x_{58}y_{18}-x_{58}r_{18})}$$

$$\psi_2 = \frac{(x_{31}(y-y_1)-y_{31}(x-x_1))(x_{74}(y-y_4)-y_{74}(x-x_4))(x_{65}(y-y_5)-y_{65}(x-x_5))}{(x_{31}y_{21}-y_{31}x_{21})(x_{74}y_{24}-y_{74}x_{24})(x_{65}y_{25}-y_{65}x_{25})}$$

$$\psi_3 = \frac{(x_{21}(y-y_1)-y_{21}(x-x_1))(x_{69}(y-y_9)-y_{69}(x-x_9))(x_{78}(y-y_8)-y_{78}(x-x_8))}{(x_{21}y_{31}-y_{21}x_{31})(x_{69}y_{39}-y_{69}x_{39})(x_{78}y_{38}-y_{78}x_{38})}$$

$$\psi_4 = \frac{(x_{85}(y-y_5)-y_{85}(x-x_5))(x_{32}(y-y_2)-y_{32}(x-x_2))(x_{31}(y-y_1)-y_{31}(x-x_1))}{(x_{85}y_{45}-y_{85}x_{45})(x_{32}y_{41}-y_{32}x_{41})(x_{31}y_{41}-y_{31}x_{41})}$$

$$\psi_5 = \frac{(x_{31}(y-y_1)-y_{31}(x-x_1))(x_{74}(y-y_4)-y_{74}(x-x_4))(x_{32}(y-y_2)-y_{32}(x-x_2))}{(x_{31}y_{51}-y_{31}x_{51})(x_{74}y_{54}-y_{74}x_{54})(x_{32}y_{52}-y_{32}x_{52})}$$

$$\psi_6 = \frac{(x_{12}(y-y_2)-y_{12}(x-x_2))(x_{47}(y-y_7)-y_{47}(x-x_7))(x_{13}(y-y_3)-y_{13}(x-x_3))}{(x_{12}y_{62}-y_{12}x_{62})(x_{23}y_{63}-y_{23}x_{63})(x_{13}y_{63}-y_{13}x_{63})}$$

$$\psi_7 = \frac{(x_{96}(y-y_6)-y_{96}(x-x_6))(x_{12}(y-y_2)-y_{12}(x-x_2))(x_{13}(y-y_3)-y_{13}(x-x_3))}{(x_{96}y_{76}-y_{96}x_{76})(x_{12}y_{72}-y_{12}x_{72})(x_{13}y_{73}-y_{13}x_{73})}$$

$$\psi_8 = \frac{(x_{69}(y-y_9)-y_{96}(x-x_9))(x_{21}(y-y_1)-y_{21}(x-x_1))(x_{23}(y-y_3)-y_{23}(x-x_3))}{(x_{69}y_{89}-y_{69}x_{89})(x_{21}y_{81}-y_{21}x_{81})(x_{23}y_{83}-y_{23}x_{83})}$$

$$\psi_9 = \frac{(x_{58}(y-y_8)-y_{58}(x-x_8))(x_{23}(y-y_3)-y_{23}(x-x_3))(x_{21}(y-y_1)-y_{13}(x-x_1))}{(x_{58}y_{98}-y_{58}x_{98})(x_{23}y_{93}-y_{23}x_{93})(x_{21}y_{91}-y_{21}x_{91})}$$

$$\psi_{10} = \frac{(x_{31}(y-y_1)-y_{31}(x-x_1))(x_{32}(y-y_2)-y_{32}(x-x_2))(x_{21}(y-y_1)-y_{21}(x-x_1))}{(x_{31}y_{10-1}-y_{31}x_{10-1})(x_{32}y_{10-2}-y_{32}x_{10-2})(x_{21}y_{10-1}-y_{21}x_{10-1})}$$